International Journal of Heat and Mass Transfer 127 (2018) 222–233

Contents lists available at ScienceDirect

International Journal of Heat and Mass Transfer

journal homepage: www.elsevier.com/locate/ijhmt

Heat transfer coefficient measurement of LN_2 and GN_2 in a microchannel at low Reynolds flow ☆

Seungwhan Baek *, Peter E. Bradley, Ray Radebaugh

Material Measurement Laboratory, National Institute of Standards and Technology, 325 Broadway, Boulder, CO 80305, USA

ARTICLE INFO

Article history:
Received 28 July 2017
Received in revised form 25 July 2018
Accepted 30 July 2018

Keywords:
Heat transfer coefficient
Microchannel
Axial conduction
Single-phase
Laminar flow
Micro-scale

ABSTRACT

The heat transfer coefficients of single-phase fluids in the laminar flow regime have been studied for decades. However, inconsistent results are found in the literature. The common finding is that the Nusselt number is dependent on the Reynolds number in the laminar flow regime, which is contrary to laminar flow heat transfer theory. Recently, researchers indicated that axial conduction in the wall of the microchannel can affect the measurement. However, there have not been thorough studies that demonstrate consistency or lack thereof between experiment and theory. This study provides an experimental investigation on heat transfer performance of gaseous and liquid nitrogen flow through microchannels with hydraulic diameters of 110 μm and 180 μm. A model has been developed to investigate heat transfer in a microchannel from which analysis shows that the temperature profile of the fluid and wall change non-linearly along the length of the microchannel when the flow rate is low (e.g., $Re < 1000$). The non-linear temperature profile conflicts with the assumption of a linear temperature profile commensurate with the traditional Nusselt number estimation method, which leads to dependency on the Reynolds number. Comparison between the experiment and numerical model of the present work validates the conclusion that the heat transfer coefficient is uniform within the laminar flow regime ($Re < 2000$) for microchannels.

1. Introduction

As microscale cooling devices are developed, the heat transfer characteristics of the fluid in the microchannels become important, with typical dimensions from 10 μm to 1 mm [1]. Microscale heat exchangers can be developed with micro-fabrication processes, which can have an extremely high heat transfer surface area per unit volume, a higher heat transfer coefficient, and a low thermal resistance. Heat transfer correlations are required to design such a heat exchanger; however, conventional forced convection heat transfer correlations were based on tubes with macro-scale dimensions. The development of heat transfer coefficient correlation for microchannels is still on-going, and has become more important due to the rapid growth in microscale cooling technology applications [2–4]. However, a heat transfer coefficient correlation for single-phase fluid flow in the laminar regime has not been developed.

Various groups have performed experimental and theoretical studies of single-phase fluid heat transfer in microchannels [5–7], but discrepancies exist among measurement results and various correlation approaches. Wu and Little [8] first measured the heat transfer coefficients of nitrogen gas flowing through micro-heat exchangers. The microchannels were prepared on silicon substrates by photolithographic technique. The hydraulic diameters of the trapezoidal microchannels were from 134 μm to 165 μm. In the laminar regime the Nusselt numbers decreased as Reynolds numbers decreased to lower values ($Re < 1000$). Later, Choi et al. [9] presented experimental data correlating Nusselt numbers with Reynolds number ranging from 50 to 10,000 in microchannels (D_h = 9.7 μm, 53 μm, and 81.2 μm). The microchannels were silica tubes with a thin polymide coating over the outer surface of the tube. They found the Nusselt numbers to be lower than theoretical values at low Reynolds flow ($Re < 2000$), and they proposed new correlations for the average Nusselt number for laminar flow. The correlation proposed by Choi et al. [9] did not agree with the experimental data by Wu and Little [8], however.

Peng and Peterson [10] measured heat transfer coefficients for water flow in microchannels. The rectangular microchannels were

☆ Contributions of NIST, not subject to copyright in the United States.

* Corresponding author at: Launcher Propulsion System Team, KSLV-II R&D Head Office, Korea Aerospace Research Institute, 169-84 Gwahak-ro, Yuseong-gu, Daejeon 34133, Republic of Korea.

E-mail addresses: sbaek@kari.re.kr (S. Baek), pbradley@nist.gov (P.E. Bradley), radebaugh@nist.gov (R. Radebaugh).

https://doi.org/10.1016/j.ijheatmasstransfer.2018.07.145
0017-9310/

Nomenclature

A	heat transfer area (m^2)
A_c	cross sectional area of fluid flow (m^2)
B	total bias error
c_p	heat capacity ($J{\cdot}kg^{-1}{\cdot}K^{-1}$)
D_h	hydraulic diameter (m)
D_i	tube inside diameter (m)
f	friction factor
G	mass flux ($kg{\cdot}s^{-1}{\cdot}m^{-2}$)
h	heat transfer coefficient ($W{\cdot}m^{-2}{\cdot}K^{-1}$)
i	enthalpy ($J{\cdot}kg^{-1}$)
k	thermal conductivity ($W{\cdot}m^{-1}{\cdot}K^{-1}$)
K	loss coefficient
L	length (m)
$\dot{m}$	mass flow rate ($kg{\cdot}s^{-1}$)
N	number of data
Nu	Nusselt number
p	pressure (Pa)
q	heat rate (W)
q''	heat flux ($W{\cdot}m^{-2}$)
Re	Reynolds number
S	standard deviation
T	temperature (K)
$t_{95\%}$	T-distribution for a confidence level
th	thickness (m)
U	uncertainty
x	length of certain point (m)

Subscripts

a	acceleration
app	apparent
exp	experimental
f	fluid, frictional
h	heating length
in	inlet
out	outlet
t	total
w	wall
x	position

Greek letters

λ	axial conduction parameter
μ	viscosity (Pa·s)
ρ	density ($kg{\cdot}m^{-3}$)
σ	contraction ratio

machined into a stainless steel plate with hydraulic diameters ranging from 150 μm to 343 μm. The dependency of the Nusselt number on the Reynolds number was found for Reynolds numbers less than 2000. They proposed an empirical correlation based on the geometric shape of the rectangular microchannel. Qu et al. [11] measured heat transfer characteristics of laminar water flow in microchannels composed of Pyrex and silicon. The experimentally derived Nusselt numbers were lower than the theoretical values, from which they concluded that the Nusselt number was related to the surface roughness. Celata et al. [12] estimated Nusselt numbers for R114 flowing in stainless steel microchannels, and also observed a reduction of the Nusselt number for the laminar flow regime. While Nusselt number appears to depend on Reynolds number for Reynolds flow less than 2000 in microchannels, none of the studies provided a clear explanation of the factors contributing to the observed reduction, and a general correlation has not been developed.

In a later work, Maranzana et al. [13] proposed an analytical heat transfer model to include the effect of axial conduction along the microchannel, and were able to describe temperature profiles that change non-linearly along the channels. This non-linearity led to a very large bias in the experimental estimation of the heat transfer coefficients, especially for low Reynolds numbers. However, precise experimental verification did not accompany the model simulations. Hetsroni et al. [14] noted that axial conduction in the wall can be significant for laminar flow. Morini et al. [15] compared Nusselt values from a thick wall microchannel to a thin wall microchannel to explain the axial conduction effect on the measurement, but the experimental data were insufficient to explain the reduction of the Nusselt number. Lin and Kandlikar [16] derived an equation to investigate the reduction of the Nusselt number by the 1st law of thermodynamics. The proposed equation was compared to available experimental data, and it was concluded that the reduction of the Nusselt number is related to the axial conduction effect.

In summary most recent studies showed significant discrepancies among experimental results and theoretical predictions. Based on recent work, consideration of the effect of axial conduction in microchannels appears to be important, but to the knowledge of the authors, direct comparisons between simulation and experimental work are not available. In the previously discussed work, the traditional Nusselt number estimation method was adopted. The traditional method measures the wall temperature at the middle of the heating section, and the inlet and outlet fluid temperatures. The fluid temperature at the middle of the heating section is calculated from the inlet and outlet fluid temperatures. It is interesting that such discrepancies are generated within similar experiments.

The purpose of this study is to highlight the discrepancies of the traditional heat transfer coefficient measurement of laminar flow in microchannels with the linear fluid temperature profile assumption. In this paper, the heat transfer coefficients of liquid and gaseous nitrogen are measured with the linear fluid temperature profile assumption. Those experimental data will be compared to the heat transfer model including the axial conduction effect. The comparison will provide a clear explanation of how the reduction of the Nusselt number is derived. In the end, the evidence of a constant Nusselt number in the laminar flow for microchannels will be provided.

2. Experimental method

The heat transfer characteristics of the gas and liquid nitrogen are examined in the microchannel. The closed-loop experimental setup enabled steady flow rate, continuous temperature and pressure measurement across the microchannel. The GM-cryocooler produced the lower temperature, which liquefies gaseous nitrogen in the closed-loop setup. The most complicated part was winding the heater and attaching thermometers on the microchannel. The following section describes the experimental setup and data reduction method.

2.1. Experiment setup

Fig. 1 displays a schematic of the experimental setup for the heat transfer coefficient measurement of a fluid in a microchannel. The closed-loop setup including a compressor, a microchannel test section, the GM-cryocooler, and a vacuum chamber is utilized for

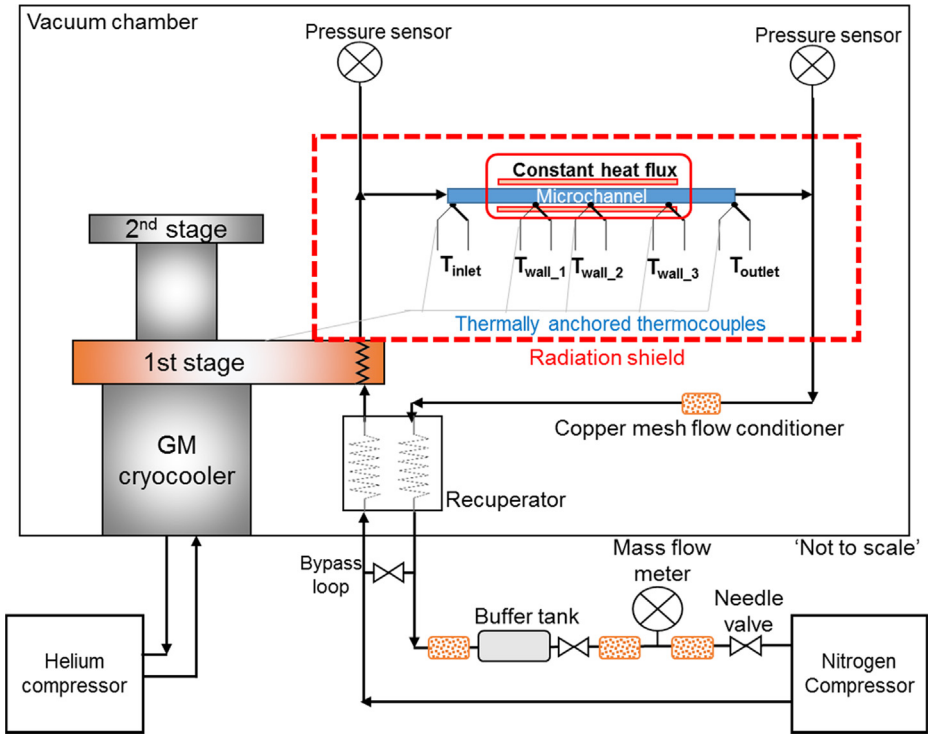

Fig. 1. The schematic of the experimental setup.

the experiment. The air-cooled, oil-less compressor is located outside the vacuum chamber. Compressed nitrogen from the compressor passes through the recuperator, then along the 1st stage of the GM-cryocooler. After passing the microchannel, it goes to the recuperator. The recuperator is a custom counterflow heat exchanger fabricated with copper tubes to reduce the heat load on the GM cryocooler. Finally, the nitrogen fluid returns to the compressor.

The test section assembled from the microchannel, heater, and several thermocouples is inserted in the test system. Table 1 describes the specifications of two microchannels for the experiment. Fig. 2(a) shows a schematic and Fig. 2(b) shows a photo of the assembled microchannel with heater. The material from which the microchannel is fabricated is stainless steel 304, although other materials can be used. Five E-type thermocouples are soldered to the microchannel wall prior to winding the heater. Thermocouples are soldered at the 25%, 50%, and 95% positions along the length of the heater to measure the wall temperature of the microchannel. The remaining thermocouples are soldered to the inlet wall and outlet wall of the microchannel to measure the inlet/outlet temperatures of the fluid.

Because the size of the thermocouple reference junction is larger than the inner diameter of the tube, thermocouples cannot be installed in the flow stream inside the microchannel. The inlet and outlet wall temperatures are assumed to be the same as the temperature of the fluid at these locations. The surface of the microchannel is cleaned with acetone after soldering the thermocouples in place. A thin layer of thermal grease is applied to the surface of the microchannel to improve the thermal contact between the heater wire and the microchannel. The heater is Evanohm wire. The heater wire is 120 μm in diameter. Once the heater wire is affixed, a conductive epoxy is applied to secure the assembly of the heater, microchannel, and thermocouple. The microchannel assembly is soldered to the metal gasket fittings that connect to copper tubes (6.35 mm OD) in the closed loop. The heater wire is electrically insulated, so there is no electrical shunt to the thermocouples or microchannels.

Fig. 3 shows a scanning electron microscopy (SEM) image of the microchannel. The inner and outer diameters for microchannels are indicated in Table 1. The roughness of the microchannel, although evident in the SEM image, was not measured in this study. The roughness effect has been known to be negligible for heat transfer in the laminar regime [17].

For thermal isolation of the test section, vacuum insulation is applied to the experimental setup. The test section is installed in a vacuum chamber maintained to better than 10^{-4} torr by a turbomolecular pump. The microchannel assembly is surrounded by a thermal radiation shield that is heat sinked to the 1st stage of the GM-cryocooler. The mass flow meter resides in the return stream to measure the flow rate of the circulating fluid. The flow rate in the closed loop is adjusted by a throttling valve at the bypass loop near the compressor. Pressure transducers are located at the entrance and exit of the microchannel to measure the pressure drop across the microchannel. Heating input to the microchannel is measured from the voltage and current supplied to the heater.

Table 1
Specifications of the stainless steel microchannel.

Microchannel	Inside diameter (μm)	Outside diameter (μm)	Total length (mm)	Heating section length (mm)	D_{in}/D_{out}
D_h = 180 μm	180 ± 2	380 ± 2	90	30	0.47
D_h = 110 μm	110 ± 2	310 ± 2	80	30	0.35

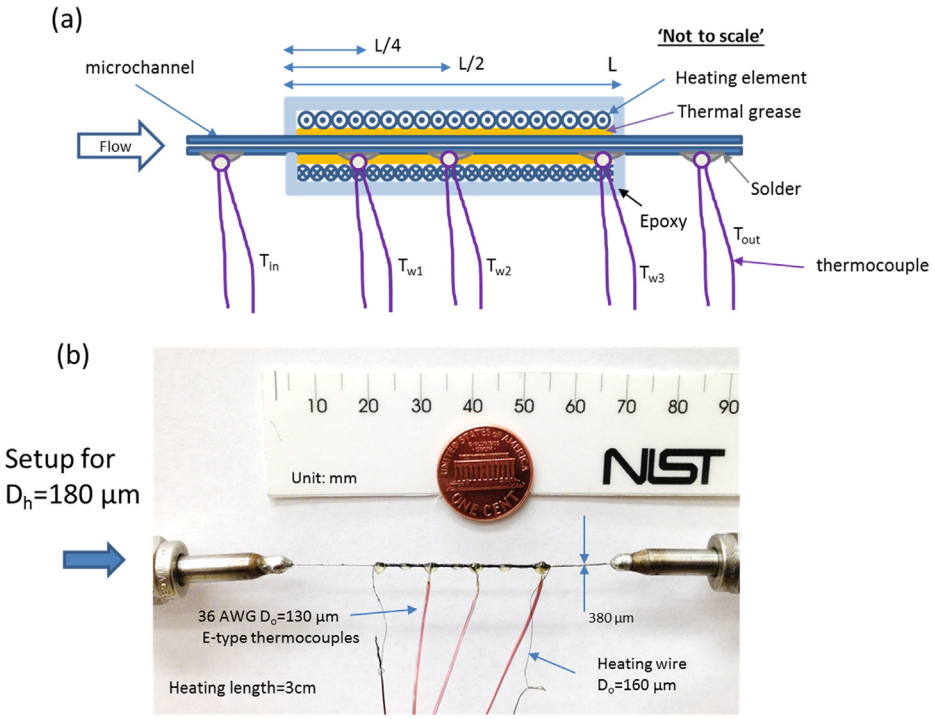

Fig. 2. (a) the schematic of the microchannel assembly with the thermocouple and heater, and (b) the photo of the microchannel assmebly.

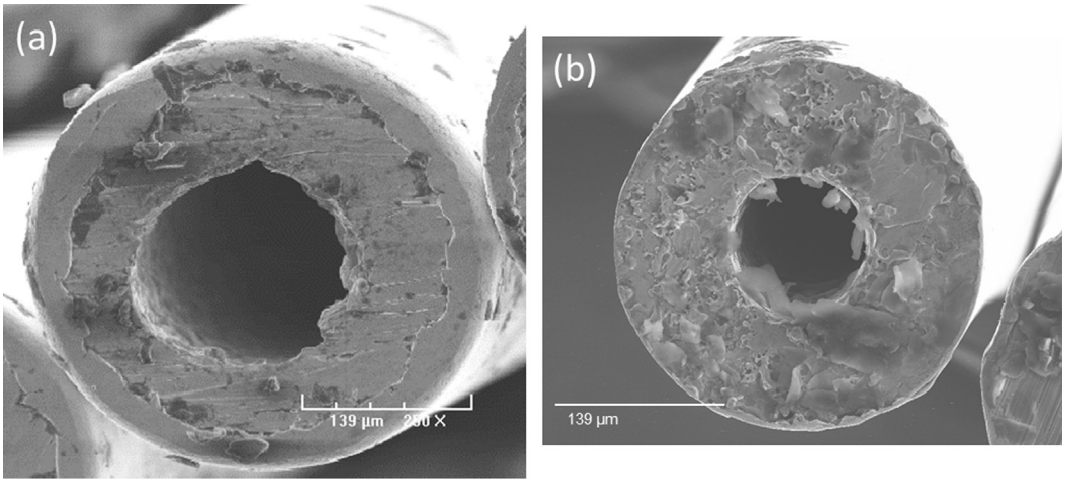

Fig. 3. The SEM image of the microchannel (a) D_h = 180 μm, and (b) D_h = 110 μm.

The additional heating elements are attached to the 1st stage of the GM cryocooler to control the temperature of the nitrogen fluid entering the microchannel. For the cryogenic experiment, the GM-cryocooler is turned on to lower the temperature of the setup. After a period of time, current is applied to the heating elements by PID-controlled power supplies to stabilize the setup to the targeted temperatures of 70 K and 150 K. Data acquisition is accomplished by Labview™ software coupled through a personal computer to collect the temperature, pressure, flowrate, and power input values to the microchannel.

2.2. Data reduction

The heat transfer coefficient of the fluid in the microchannel is estimated by the traditional method, as described by Maranzana et al. [13], Morini et al. [15], and Yang et al. [18]. The heat transfer rate q, is measured from the DC power input deduced by the corresponding calibrated heat loss. The results equal the increased enthalpy of the nitrogen flow. Usually it is assumed that the heat is added uniformly along the tube surface. Therefore, the local fluid temperature, $T_{f,x}$, at a position x from the heating entrance can be estimated by the assumption of a linear temperature profile along the inside of the channel:

$$q\frac{x}{L_h} = \dot{m}c_p(T_{f,x} - T_{in}) = \dot{m}(i_x - i_{in}), \tag{1}$$

where $\dot{m}$ is the mass flow rate, c_p is the heat capacity of the fluid, L_h is the channel heating length, and T_{in} is the inlet temperature. The term i is the enthalpy at each position, which can be estimated from an equation of state from the measured temperature and pressure. Because the fluid temperature profile is assumed linear, the fluid

temperature at the middle position of the channel can also be estimated from the inlet and outlet temperatures as follows:

$$T_{f,50\%} = \frac{T_{f,in} + T_{f,out}}{2}. \quad (2)$$

From Newton's law of cooling, the following equation is derived as

$$q'' = \frac{q}{A} = h(T_{w,x} - T_{f,x}). \quad (3)$$

Therefore, the local heat transfer coefficient h at a certain position x can be derived as

$$h_x = \frac{q}{A(T_{w,x} - T_{f,x})}, \quad (4)$$

where A is the heat transfer area, $A = \pi D_i L_h$, and D_i is the inside diameter of the tube. The term $T_{w,x}$ is the inside local tube surface temperature that can be inferred from the thermocouples located outside the tube. The Reynolds number is defined as follows:

$$Re = \frac{GD_h}{\bar{\mu}} \quad (5)$$

where G is the flow mass flux defined as $G = \dot{m}/A_c$, A_c is the cross-sectional area of flow in the tube, and the viscosity ($\bar{\mu}$) of the fluid is the average value corresponding to the inlet and outlet. The viscosity is calculated from REFPROP [19]. The Nusselt number is defined as

$$Nu_x = \frac{h_x D_h}{\bar{k}_f}, \quad (6)$$

where $\bar{k}_f$ is the thermal conductivity of the fluid, which is the average value from the inlet and outlet of the microchannel. The data are gathered every few seconds and time-averaged for a minute. The uncertainty of the measured data is determined with Eq. (7) [11], where B is the total bias error, N is the total number of data, and S is the standard deviation of the data. $t_{95\%}$ is 2.000 in this case.

$$U = \sqrt{B^2 + \left(t_{95\%}\frac{S}{\sqrt{N}}\right)} \quad (7)$$

Table 2 shows the error of the measurement and the total uncertainty of the Nusselt number. The experimental results show an uncertainty of around 7%.

3. Experimental results and discussion

The analysis of experimental measurements such as mass flow rate, temperature and pressure has been conducted to calculate friction factors and Nusselt numbers. These values compared to the theoretical values.

3.1. Friction coefficients

The pressure drop across the channel is measured to find friction factors for microchannels. The comparison of experimental and theoretical friction factors can distinguish the roughness effect, and confirm the validity of the macrochannel theory to microchannels. The total fluid flow pressure drop, Δp_t, is measured at the condition of no added heat input. The frictional pressure drop Δp_f. is evaluated by subtracting the inlet, exit, and acceleration terms from the measured total pressure drop:

$$\Delta p_f = \Delta p_t - \Delta p_{in} - \Delta p_{out} - \Delta p_a. \quad (8)$$

The pressure losses at the inlet Δp_i, at the exit Δp_e, and the acceleration term Δp_a. are calculated by following relations suggested by Kays and London [20]:

$$\Delta p_{in} = \frac{G^2}{2\rho_{in}}(1 - \sigma^2 + K_{in}), \quad (9)$$

$$\Delta p_{out} = \frac{G^2}{2\rho_{out}}(1 - \sigma^2 + K_{out}), \quad (10)$$

$$\Delta p_a = \frac{G^2}{2\rho_{in}}\left(\frac{\rho_{in}}{\rho_{out}} - 1\right). \quad (11)$$

The term σ is the test section connector's contraction ratio and K_{in}, and K_{out} are the entrance and exit loss coefficients which are obtained from Kays and London correlations [20]. The experimental Fanning friction coefficients are derived directly from

$$f = \frac{\rho D_h \Delta p_f}{2G^2 L}. \quad (12)$$

Fig. 4 displays the measured Fanning friction factors at various Reynolds numbers. The measured inner diameter from the SEM is used as the hydraulic diameter in Eq. (12). The theoretical friction factor in the laminar flow regime is also plotted in Fig. 4. The theoretical friction factor for the laminar flow can be calculated from

$$f_{theory} = \frac{16}{Re}. \quad (13)$$

The comparison results between the experimental and theoretical friction factors show good agreement. The comparison also implies that the roughness effect is negligible.

3.2. Nusselt numbers

The heat transfer coefficient for nitrogen flow in the microchannel is estimated from the measured wall temperature at the middle of the heated length ($T_{w,50\%,exp}$), and the fluid temperature at the middle of the channel ($T_{f,50\%}$), which is calculated with Eq. (1) derived under the assumption of a linear temperature profile when wall thermal conduction is ignored. Fig. 5 displays the estimated

Table 2
Characteristics and uncertainties of the measurement instruments.

Measurement	Range	Error
Temperature	77–300 K	±0.1 K
Pressure	0–1 MPa	±0.5%
Mass flow rate	0–500 sccm	±0.5%
Total uncertainty		~7%

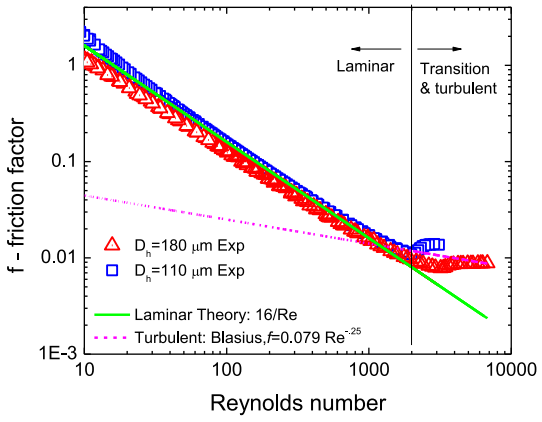

Fig. 4. The Fanning friction factor of the microchannel.

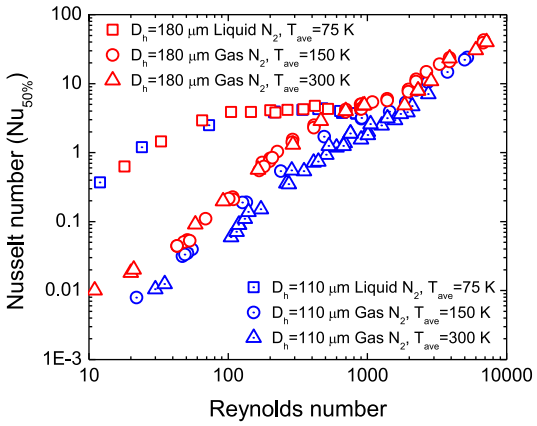

Fig. 5. Experimental Nusselt number based on the traditional Nusselt number estimation.

Nusselt numbers using this assumption according to the various Reynolds numbers for different microchannels and temperatures.

The results for D_h = 180 μm are indicated as red hollow figures. For the gas experiment around 300 K, the inlet temperature is maintained at approximately 296 K. The estimated Nusselt numbers become as small as 0.01 when the Reynolds number is decreased to 10. The Nusselt number results show similar values to a theoretical value of 4.36 for Reynolds numbers between 1000 and 2000. For Reynolds numbers larger than 2000, the Nusselt number increases because it follows the heat transfer characteristic consistent with turbulent flow. These results are consistent with previous results from Morini et al. [15], Wu and Little [8], Celata et al. [21], and Choi et al. [9], which show Nusselt number dependences on the Reynolds numbers for the laminar flow regime.

Heat transfer measurements were also made around 150 K with the 180 μm tube. For these cases, the inlet temperature is maintained at approximately 110 K, which results in an average of ~150 K along the microchannel. For the gas experiment at 150 K, the Nusselt numbers show values similar to those estimated at 300 K. The physical property change of nitrogen is small between 150 K and 300 K, however. Thus, there is no significant difference between these two experimental results at 150 K and 300 K.

The Nusselt numbers with liquid nitrogen flow in the microchannel are also estimated for D_h = 180 μm. In this instance, the inlet temperature is maintained at 67 K which gives an average of ~70 K for the microchannel. Estimated Nusselt numbers are displayed in Fig. 5, and they tend to show a theoretical value of 4.36 when the Reynolds number is larger than 100. When the Reynolds number is less than 100, the measured Nusselt numbers decreased to 0.6 as Reynolds numbers decreased to 20. The reduction of Nusselt numbers with liquid flow is also found in the literature. Hetsroni et al. [22] also observed such a behavior with water flow in microchannels. However, the estimated Nusselt numbers show significant differences from those with gas experiments.

Another set of experiments has been performed with the D_h = 110 μm tube at 70 K, 150 K and 300 K. For the 300 K experiment, the Nusselt numbers show lower values than for the D_h = 180 μm tube. The 150 K experimental results for D_h = 110 μm show slightly higher values than those at 300 K; however, the difference is small as shown in Fig. 5. The Nusselt number for liquid nitrogen for D_h = 110 μm tube shows an almost identical trend as with the D_h = 180 μm tube for which a nonlinear relation is observed. The estimated Nusselt numbers from experiment show a theoretical value of 4.36 compared to a Reynolds number of 100, and Nusselt numbers decrease to 0.4 when the Reynolds number is 10.

The major difference between the two microchannels is the ratio of inner and outer diameters. The D_h = 110 μm tube has a thicker wall than the D_h = 180 μm tube. This difference may cause the Nusselt number difference in the gas experiment. Previous researchers mentioned axial conduction effects in heat transfer measurements [13,15,23]. They explained that the fluid temperature profile becomes non-linear due to the axial conduction effect. Therefore, an inconsistency exists between reality and assumptions during the data reduction process. Maranzana et al. [13] employed an analytical solution that showed the temperature profile becomes non-linear. However, a direct comparison with experiment was not performed. In the next section, a model is developed to simulate the heat transfer in the microchannel in the presence of tube axial conduction.

4. Modeling of heat transfer in microchannels

4.1. Development of heat transfer model with axial conduction: a numerical approximation

A simulation model has been developed to describe heat transfer phenomena in microchannels. A one-dimensional microchannel heat transfer model that includes the axial conduction effect was developed in MATLAB™. The model is composed of a fluid channel and two surrounding walls, as displayed in Fig. 6. The numerical technique proceeds by identifying control volumes and placing nodes at locations for which the temperature will be predicted. One arrangement of nodes and control volumes is shown in Fig. 6. The numerical solution is enabled by carrying out an energy balance on each of the control volumes identified in this figure. The governing equations are developed for an energy balance based for (1) fluid streams and (2) channel walls, respectively, Eqs. (14) and (15), as follows:

$$\dot{m}c_p\frac{dT_f}{dx} = -\left(\frac{h_1A_{HT,1}}{L}\right)(T_f - T_{w,1}) - \left(\frac{h_2A_{HT,2}}{L}\right)(T_f - T_{w,2}) \tag{14}$$

$$\frac{d}{dx}\left(k_{w,1}A_{c,w,1}\frac{dT_{w,1}}{dx}\right) + \frac{d}{dx}\left(k_{w,2}A_{c,w,2}\frac{dT_{w,2}}{dx}\right) = \dot{m}c_p\frac{dT_f}{dx} \tag{15}$$

The numerical scheme for a similar heat transfer model with axial conduction is fully described by Nellis and Klein [24], and Baek [25]; thus, only important details will be highlighted in this paper. The model inputs are as follows:

- heat transfer coefficients between the wall and fluid (h)
- thickness (th_w) and thermal conductivity (k_w) of the wall
- mass flow rate ($\dot{m}$), inlet temperature (T_{in}), heat capacity (c_p), and thermal conductivity (k_f) of the fluid
- channel height (D_h), width (W), heated length (L)
- heat transfer area (A_{HT}), and cross-sectional area of channel ($A_{c,w}$) calculated from the channel geometry
- heat input to the channel (q)

The pressure drop in the microchannel is neglected in this numerical model, because the thermophysical property differences are negligible for the pressure change in laminar flow. The thermal resistance of the metal and fluid is also neglected. The axial conduction in the fluid is ignored where it is relatively negligible compared to the axial conduction through the metal heat transfer medium. The heat capacity (c_p), thermal conductivity (k_f) of the fluid assumed to have constant values in the microchannel. The heat transfer coefficient (h) is assumed to be constant throughout the channel.

The output results from the microchannel heat transfer model are the temperature profiles of the fluid and the wall. Because

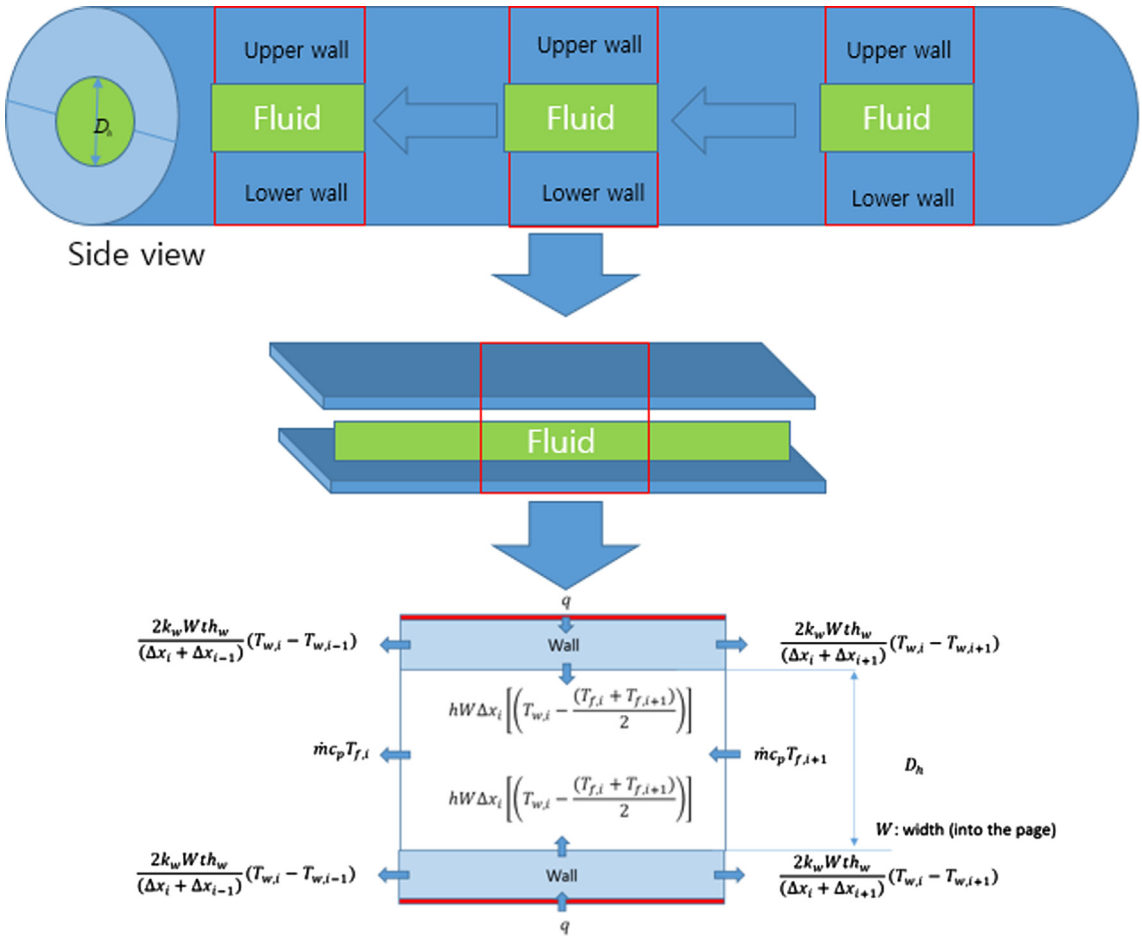

Fig. 6. Finite element heat transfer model in the microchannel.

the inlet and outlet temperature are solved from the model, the identical data reduction procedure from Section 2.2 can be applied to derive a Nusselt number. For estimation of the Nusselt number, the calculated wall temperature at 50% of the channel length is used, and the fluid temperature is calculated with Eq. (2).

This model is compared to available literature results to validate its applicability under different operating conditions. Results from the present model are compared to solutions from Maranzana et al. [13] and Lin et al. [16] (Fig. 7) for water flow in a 100 μm channel formed by two 10 mm long and 500 μm thick silicon blocks. The thermal conductivity of the material is set as $k_w = 135\ \mathrm{W{\cdot}m^{-1}{\cdot}K^{-1}}$ and the thermal conductivity of water is $k_f = 0.63\ \mathrm{W{\cdot}m^{-1}{\cdot}K^{-1}}$. The channel is heated by a $30\ \mathrm{kW{\cdot}m^{-2}}$ heat flux on one wall, and the other wall has an adiabatic boundary condition applied. A uniform heat transfer coefficient is assumed, from the constant Nusselt number of 4.12 for the rectangular channel.

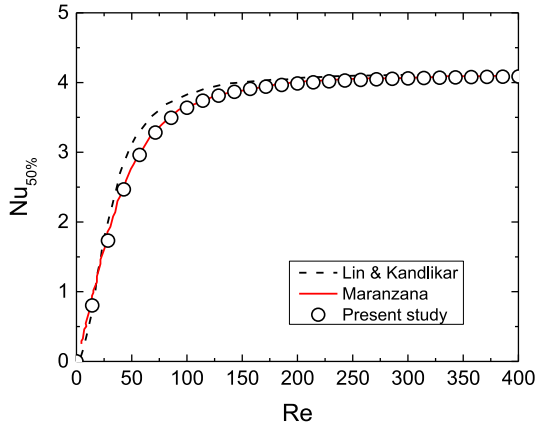

Fig. 7. Comparison of calculation between the present model and preceding results for a case in which wall thermal conduction cannot be neglected at low Re.

Fig. 7 shows the numerical simulation results for the apparent Nusselt number by Maranzana et al. [13] and Lin & Kandlikar [16] plotted as $Nu_{50\%}$ versus *Re*. The present model is also plotted in Fig. 7. Present model results agree well with the analytic solution of Maranzana et al. [13].

4.2. Model calculation results

The numerical model is used to demonstrate heat transfer for the microchannel used for the experiments. The geometry and property values used in the model are summarized in Table 3. The heat transfer coefficient between the wall and the fluid is calculated for a Nusselt number of 4.36. A uniform heat transfer coefficient to the wall is assumed and applied to the model, as the study by Maranzana et al. [13] did. An axial conduction parameter is introduced here to demonstrate the effect of axial conduction to the temperature profile of the wall and fluid. The axial conduction parameter λ is defined from the heat exchange length (L_h), cross sectional area of the wall (A_w), the thermal conductivity of the wall (k_w), and the heat capacity rate ($\dot{m}c_p$) in the following equation:

Table 3
Model input.

Geometry and property	Value
Diameter of the channel	D_h = 180 μm, 110 μm
Width of the channel	$W = D_h/2 * \pi$
Thickness of the wall	th_w = 100 μm
Thermal conductivity of wall	k_w = 16 W·m^{-1}·K^{-1} @ 300 K
	k_w = 10 W·m^{-1}·K^{-1} @ 150 K
	k_w = 6 W·m^{-1}·K^{-1} @ 70 K
Thermal conductivity of fluid	k_f = 0.025 W·m^{-1}·K^{-1} @ 300 K
	k_f = 0.014 W·m^{-1}·K^{-1} @ 150 K
	k_f = 0.145 W·m^{-1}·K^{-1} @ 70 K
Viscosity of fluid	$\bar{\mu}$ = 17 ×10^{-6} Pa-s
	$\bar{\mu}$ = 10 ×10^{-6} Pa-s
	$\bar{\mu}$ = 164.95 × 10^{-6} Pa-s
Heat capacity of fluid	c_p = 1047 kJ·kg^{-1}·K^{-1}
	c_p = 1089 kJ·kg^{-1}·K^{-1}
	c_p = 2024 kJ·kg^{-1}·K^{-1}
Heat input to wall	0.1 W
Nusselt number	Nu = 4.36

$$\lambda = \frac{k_w A_w}{L_h \dot{m} c_p} \tag{16}$$

Fig. 8(a) and (b) show the temperature profiles of the wall and the fluid in the microchannel for two different case studies. The temperature profiles are non-dimensionalized with respect to the fluid inlet and outlet temperature as expressed in

$$T(\Theta) = \frac{T_{x(wallorfluid)} - T_{f,in}}{T_{f,out} - T_{f,in}}. \tag{17}$$

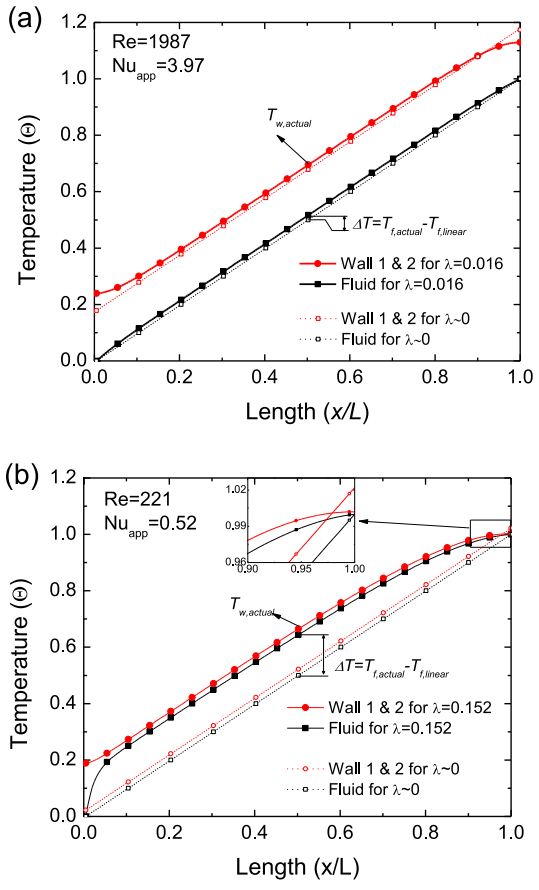

Fig. 8. Simulated temperature profile of wall and gaseous nitrogen in the microchannel (a) when the axial conduction effect is small (λ = 0.016), and (b) when the axial conduction effect is large (λ = 0.152).

Fig. 8(a) shows the temperature profile of the wall and fluid when Re = 1981, and the axial conduction parameter (λ) is 0.016. This case simulates a nearly transitional flow condition with a very small axial conduction effect. Usually, the axial conduction effect can be considered negligible if the conduction parameter is less than 0.01 [26]. When the axial conduction effect is completely negligible ($\lambda \sim 0$), the temperature profile of the wall and fluid exhibit a perfect linear profile, shown by dotted lines. Linear temperature profiles are assumed for the traditional calculations of the Nusselt number. However, when axial conduction is considered, the temperature profile of the wall and fluid exhibits a distinctly non-linear profile particularly at the entrance and exit, shown by solid red lines in Fig. 8(a). The temperature difference (ΔT) is found in Fig. 8 between the non-axial conduction condition and the axial conduction effected condition.

An apparent heat transfer coefficient and an apparent Nusselt number can be defined when axial conduction is considered. The apparent heat transfer coefficient can be estimated from the traditional Nusselt number data reduction method explained in Section 2.2. The wall temperature at the middle of the channel from the calculation is used, and the fluid temperature at the middle of the channel is calculated from Eq. (2). The total heat input (Q) and the total heat transfer area (A) is utilized to estimate the heat transfer coefficient for Eq. (4). The value of the apparent heat transfer coefficient (h_{app}) may be defined as follows:

$$h_{app,50} = \frac{Q}{A(T_{w,50} - T_{f,50,linear})}. \tag{18}$$

The apparent Nusselt number can now be estimated, accordingly from

$$Nu_{app,50} = \frac{h_{app,50} D_h}{\bar{k}_f}. \tag{19}$$

Eq. (19) is defined with the apparent heat transfer coefficient, and it has the subscript of 'app' to indicate that this value does not represent the actual Nusselt number. Because the temperature difference exists between the linearly assumed fluid temperature profile and the non-linear fluid temperature profile, the term $T_{w,50} - T_{f,50,linear}$ is larger than $T_{w,50} - T_{f,50,non\text{-}linear}$. Therefore h_{app} becomes smaller than h_{actual}. Consequently, Nu_{app} becomes smaller due to the decreased value of h_{app}. For the case in Fig. 8(a), the Nu_{app} is 3.97, which is less than the theoretical value of 4.36. Although the Reynolds number is almost 2000, the reduction of the Nusselt number occurs due to the inaccurate assumption of a linear fluid temperature profile.

Fig. 8(b) shows a case with a much lower Reynolds number of Re = 221 and a higher axial conduction parameter of λ = 0.152. The temperature profile of the wall and fluid for the axial conduction condition (λ = 0.152) and zero axial conduction condition ($\lambda \sim 0$) are presented in the figure. The wall and fluid temperature profile of the axial conduction condition is much higher than that of the non-axial conduction condition due to the higher axial conduction parameter (λ). The fluid temperature increases significantly at the inlet of the channel, and then, exhibits a similar trend to the wall-temperature profile. At the outlet of the channel, the fluid temperature closely approaches the wall temperature. The Nusselt number can be also estimated for the case Fig. 8(b) with Eqs. (18) and (19), and it results in Nu_{app} = 0.52. The larger temperature difference of $T_{w,50} - T_{f,50,linear}$ results in a much lower apparent Nusselt number than that for the theoretical value.

The simulation is also performed with liquid nitrogen with the same geometry of the tube. Fig. 9 shows the temperature profile of the wall and fluid for different axial conduction parameters (λ) and Reynolds numbers. Fig. 9(a) shows the temperature profile of the liquid nitrogen and wall when Re = 452. The axial conduction

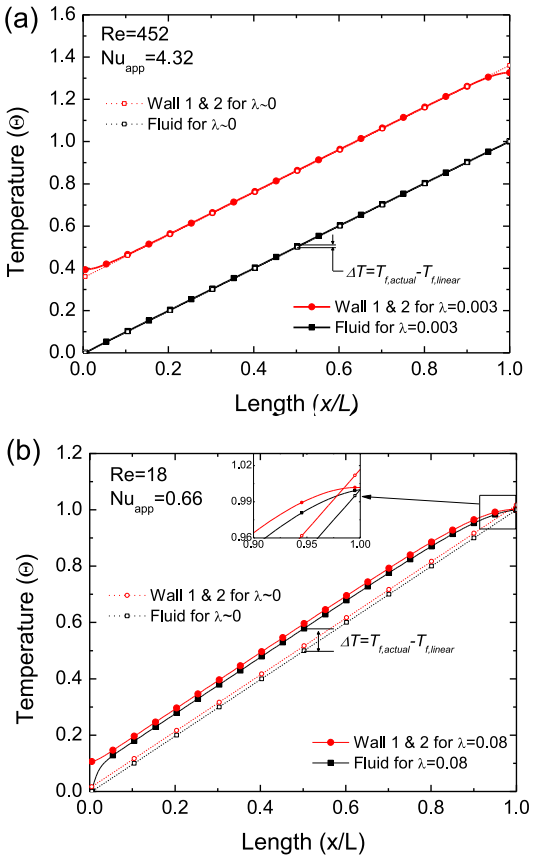

Fig. 9. Simulated temperature profile of the wall and liquid nitrogen in the microchannel (a) when the axial conduction effect is small (λ = 0.003), and (b) when the axial conduction effect is large (λ = 0.08).

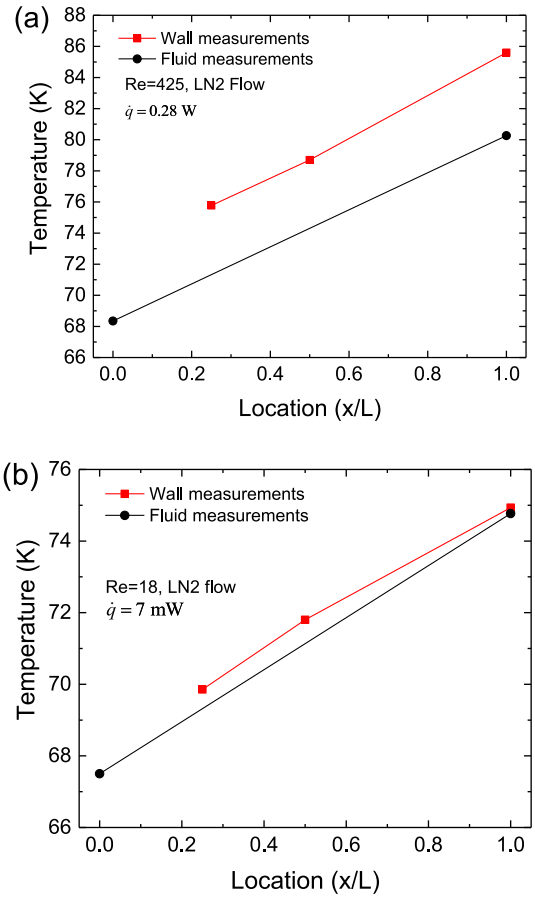

Fig. 10. Experimental temperature profile of wall and fluid in the microchannel (a) LN2 flow in the D_h = 180 μm channel, Re = 425 (b) LN2 flow in the D_h = 180 μm channel, Re = 18. Dots are connected with straight lines.

parameter (λ) is much lower at 0.003 than gas flowing condition. The heat capacity of liquid nitrogen is a factor of two larger than for gaseous nitrogen; therefore, the axial conduction parameter becomes smaller. Also, the much higher viscosity of the liquid makes the Reynolds number lower for the same mass flow rate. Nu_{app} is calculated as 4.32 where it is almost identical to the theoretical value. Fig. 9(b) shows the temperature profile of the wall and liquid nitrogen when Re = 18. The axial conduction parameter is 0.08. In this case, the axial conduction affects the temperature profile. Non-linear temperature profiles are observed at the inlet and outlet of the channel. Nu_{app} is calculated as 0.66 in this case.

The experimentally measured wall temperatures and fluid temperatures are indicated in Fig. 10(a) and (b). Fig. 10(a) shows the case of liquid nitrogen flow when Re = 425. The wall and fluid temperature profiles show linear profiles as shown in Fig. 9(a). The wall and fluid temperature profiles also show a distinguishable difference with each other. However, when the Reynolds number is as low as 18, the gap between the wall and fluid temperatures becomes smaller as indicated in Fig. 10(b). The experimental measurement shows an identical trend with simulations as shown in Fig. 9(b).

Fig. 11 displays a simulated heat flux density along the length for four cases discussed above. For the case when the axial conduction is not significant (high Reynolds and low axial conduction effect), the heat flux values are slightly higher than the uniform heat flux at the inlet with correspondingly lower values at the outlet, as indicated with the red circle line in Fig. 11(a) and (b). However, for a much lower Reynolds flow and significant axial conduction, the heat flux values at the inlet are higher than the uniform heat flux and gradually decrease along the length, whereas the heat flux converges to zero (black square line in Fig. 11(a) and (b)). Because the heat flux becomes very small at the outlet, the wall and fluid temperatures approach each other for this case.

Apparent Nusselt number calculations from the present model have been performed for varying Reynolds numbers employing liquid and gaseous nitrogen flow in microchannels. Fig. 12(a) and (b) display the model calculation results for D_h = 180 μm and 110 μm, respectively. The calculated apparent Nusselt number for 70 K liquid nitrogen only shows a reduction for Re values less than 100. The calculated apparent Nusselt number for 300 K nitrogen gas exhibits a large dependence on the Reynolds number (Re < 1000). The calculated apparent Nusselt number for 150 K nitrogen gas shows an identical trend.

Simulated apparent Nusselt numbers show good agreement when compared with the experimental values for Reynolds flow less than 2000 in Fig. 12. The Nusselt values for turbulent flow, as calculated from the Dittus-Boelter equation [27], are plotted in Fig. 12. Experimental Nusselt values show good agreement, where mean average percentage error (MAPE) shows 33%,with the Dittus-Boelter equation when Reynolds values are greater than 2000. The Eq. (20) shows the definition of MAPE. The value n is the number of sample, y_m is the measured value, y_p is the predicted value of i-th sample. Fig. 13 shows the discrepancies between measured and predicted values.

$$MAPE = \frac{1}{n}\sum_{i=1}^{n}\left|\frac{y_m - y_p}{y_m}\right|_i \times 100 \qquad (20)$$

For turbulent flow, the axial conduction effect becomes negligible (λ<0.01). Therefore, estimation of heat transfer coefficients employing the linear temperature profile can be applied. For Re <

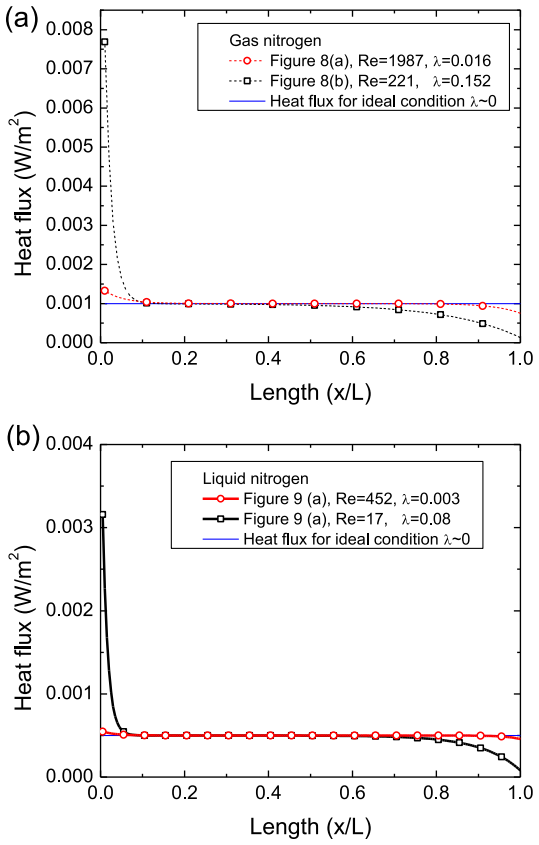

Fig. 11. Simulated Heat flux along the length for difference cases: (a) gaseous nitrogen, and (b) liquid nitrogen.

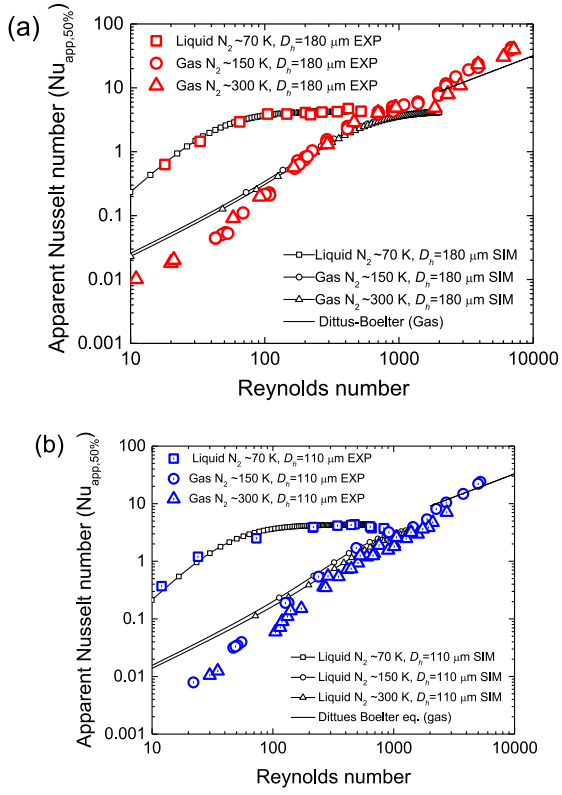

Fig. 12. Comparison of apparent Nusselt number between the model and the experiment.

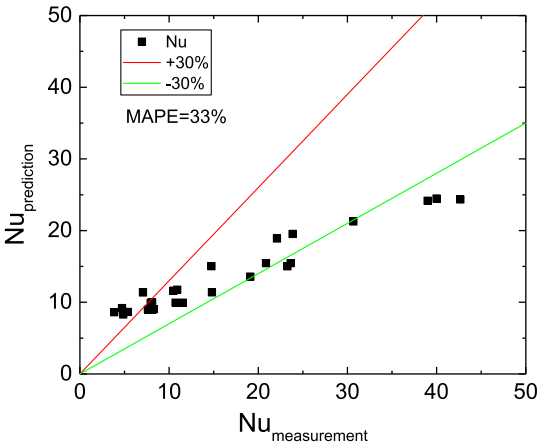

Fig. 13. The Nusselt number measurement in the turbulent regime (Re > 2000), and its comparison to the Dittus-Boelter equation. The MAPE shows 33% discrepancy.

2000, experimentally determined apparent Nusselt numbers follow the trend of the simulated apparent Nusselt numbers for GN_2 and LN_2. As a uniform heat transfer coefficient is assumed in the model, a comparison indicates that this assumption is also valid for the experiment. Consequently, a constant Nusselt number therefore holds for the fully developed laminar flow.

As discussed above, the estimation of the Nusselt number based on a linear temperature profile of the wall and fluid leads to inaccurate estimations, which in turn lead to erroneous conclusions. Most previous research assumed a linear temperature profile, from which a Nusselt number dependence on Reynolds number was concluded for laminar flow of $Re < 2000$. For accurate heat transfer coefficient measurements when the axial conduction is considered, a non-linear fluid temperature profile inside the microchannel should be measured. In most instances, the thermometer size is larger than the flow section within the microchannel, thereby limiting direct measurement of the fluid in the channel. This limitation has led to estimating the temperature profile by inaccurately assuming linearity of the fluid temperature along the channel. However, measurement of the temperature inside the channel may be possible by non-intrusive methods such as by infra-red or other laser spectroscopy as reported by other researchers [13,18,28,29].

5. Heat transfer coefficient analysis by wall temperature slope

As discussed above, estimation of the actual heat transfer coefficient with the traditional method is not appropriate. Therefore, an alternative estimation of the heat transfer coefficient is required when the axial conduction effect is dominant. The wall temperatures of three different locations were measured on the microchannel, and this additional information can be used for the heat transfer coefficient analysis. The usefulness of the information is evaluated by numerical calculation with the developed model.

Because the measurement condition is dominated with the axial conduction effect, the model is modified to simulate the actual experimental condition. A no heating zone is added before and after the heating zone. The total length of the simulated length is 500 mm, and the heating zone length is 300 mm, which is identical to the experimental condition. Fig. 14 displays the non-dimensional wall-temperature profiles when the Reynolds number is 109 with the D_h = 180 μm tube. The Nusselt number is changed from 4.36 to 0.1. When the Nusselt number is as low as 0.1, the non-dimensional wall temperature is high, because the heat is barely transferred to the fluid. In contrast, the non-dimensional

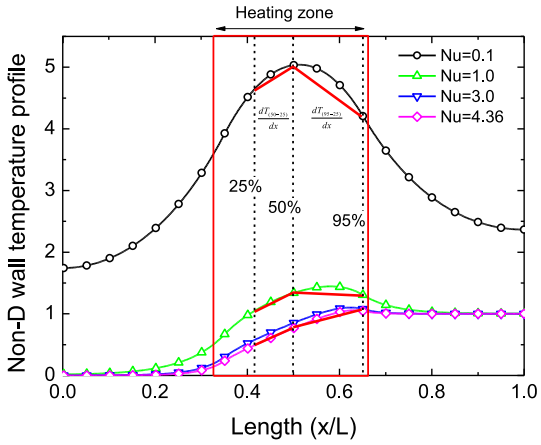

Fig. 14. Non-dimensional wall temperature profile when $Re = 109$ with gas nitrogen in $D_h = 180$ μm microchannel.

wall temperatures show values around 1 when the Nusselt number is as high as 4.36. This value indicates that the wall temperatures are similar to the fluid temperatures. From Fig. 14, the non-dimensional wall temperature slopes can be also analyzed. The slopes from 25% to 50% ($\frac{dT_{(50-25)}}{dx}$), and 50% to 95% $\left(\frac{dT_{(95-50)}}{dx}\right)$ are with thick red-lines indicated for different Nusselt numbers in Fig. 14. The average slope can be calculated with

$$\frac{dT_{ave}}{dx} = \left(\frac{dT_{(50-25)}}{dx} + \frac{dT_{(95-50)}}{dx}\right) \Big/ 2 \tag{21}$$

As seen from Fig. 14, the average slope shows a lower value when the Nusselt number is low, and the average slope increases as the Nusselt number increases. Therefore, these average slope values can be used for the Nusselt number analysis. Fig. 15 shows the non-dimensional average wall temperature slopes for different Reynolds numbers and Nusselt numbers. Fig. 15(a) shows the case for gaseous nitrogen in the $D_h = 180$ μm tube. The average slope when $Nu = 0.1$ is significantly lower than that for $Nu = 4.36$. The experimental average slopes are also indicated in Fig. 15(a). The graph indicates that experimental values lie above $Nu = 4.36$ when the Reynolds number is around 100. This means that the actual Nusselt number is around 4.36 when the Reynolds number is as low as 100. The interpretation is totally different from Fig. 12, where the apparent Nusselt number is around 0.1 for gaseous nitrogen. The heat transfer phenomena with a Nusselt number of 0.1 are not physically meaningful. Fig. 15(b) shows the slope comparisons for liquid nitrogen. The experimental average slope data are situated above the $Nu = 4.36$ line when the Reynolds number is larger than 10, implying that the actual Nusselt number is around 4.36 considering the effect of axial conduction.

When the Reynolds number is extremely low and the axial conduction effect is dominant with a constant wall heat flux, the wall-temperature profile becomes almost flat for a constant wall-temperature condition. At this extreme case, the Nusselt number may converge to a value of 3.66 rather than 4.36. The current measurement method for the heat transfer coefficient is limited due to the fluid temperature measurement in the microchannel. Therefore, for an improved estimation of the heat transfer coefficient, the fluid temperature in the microchannel should be measured directly.

6. Conclusion

This study provides an experimental and numerical investigation into the pressure drop and the heat transfer performance of

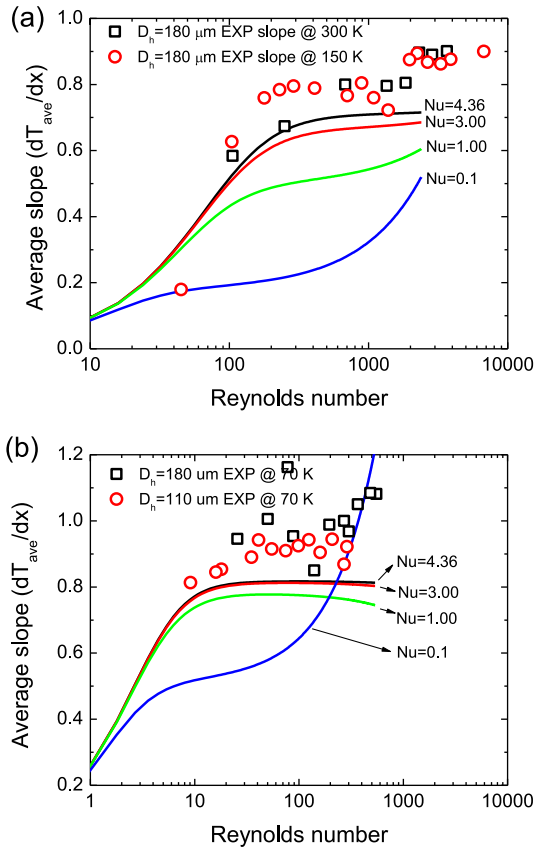

Fig. 15. Comparison of the wall temperature slope along the length between the experiment and the model calculation (a) for gaseous nitrogen, and (b) for liquid nitrogen.

nitrogen flow through microchannels with hydraulic diameters of 180 μm and 110 μm. The experimental results show that the friction coefficient of gaseous flow in microchannels is the same as that in conventional macro-scale tubes. A numerical model developed to simulate the heat transfer in microchannels, showed that axial conduction through the wall results in non-linear temperature profiles of the wall and fluid concluding that a non-linear heat flux to the fluid is present in the axial direction of the microchannel. Calculation of Nusselt numbers based on assumed linear temperature profiles results in the apparent dependency of the Nusselt number on the Reynolds number seen in recent literature at low laminar flows. It was also shown that a uniform heat transfer coefficient is valid for laminar flow conditions in microchannels of this work. The wall-temperature slope comparison between calculation and experiment indicates that the actual Nusselt number is around 4.36, which differs from the apparent Nusselt number.

Conflict of interest

The authors declared that there is no conflict of interest.

Acknowledgement

We gratefully acknowledge DARPA FPA-MCC program for funding support.

References

[1] T. Dixit, I. Ghosh, Review of micro- and mini-channel heat sinks and heat exchangers for single phase fluids, Renew. Sustain. Energy Rev. 41 (2015) 1298–1311.

[2] R. Radebaugh, Thermodynamic analysis of cascade microcryocoolers with low pressure ratios, AIP Conf. Proc. 1573 (1) (2014) 132–141.
[3] Q. Li, G. Flamant, X. Yuan, P. Neveu, L. Luo, Compact heat exchangers: A review and future applications for a new generation of high temperature solar receivers, Renew. Sustain. Energy Rev. 15 (9) (2011) 4855–4875.
[4] S. Baek, J.-H. Kim, S. Jeong, J. Jung, Development of highly effective cryogenic printed circuit heat exchanger (PCHE) with low axial conduction, Cryogenics 52 (7–9) (2012) 366–374.
[5] B.H. Salman, H.A. Mohammed, K.M. Munisamy, A.S. Kherbeet, Characteristics of heat transfer and fluid flow in microtube and microchannel using conventional fluids and nanofluids: a review, Renew. Sustain. Energy Rev. 28 (2013) 848–880.
[6] M. Asadi, G. Xie, B. Sunden, A review of heat transfer and pressure drop characteristics of single and two-phase microchannels, Int. J. Heat Mass Transf. 79 (2014) 34–53.
[7] G.L. Morini, Single-phase convective heat transfer in microchannels: a review of experimental results, Int. J. Therm. Sci. 43 (2004) 631–651.
[8] P. Wu, W.A. Little, Measurement of the heat transfer characteristics of gas flow in fine channel heat exchangers used for microminiature refrigerators, Cryogenics 24 (1984) 415–420.
[9] S. Choi, R. Barron, R. Warrington, Fluid flow and heat transfer in microtubes, ASME DSC (1991) 123–134.
[10] X.F. Peng, G.P. Peterson, Convective heat transfer and flow friction for water flow in microchannel structures, Int. J. Heat Mass Transf. 39 (12) (1996) 2599–2608.
[11] W. Qu, G.M. Mala, D. Li, Heat transfer for water flow in trapezoidal silicon microchannels, Int. J. Heat Mass Transf. 43 (21) (2000) 3925–3936.
[12] G.P. Celata, M. Cumo, M. Guglielmi, G. Zummo, Experimental investigation of hydraulic and single-phase heat transfer in 0.130-mm capillary tube, Microscale Thermophys. Eng. 6 (2) (2002) 85–97.
[13] G. Maranzana, I. Perry, D. Maillet, Mini- and micro-channels: influence of axial conduction in the walls, Int. J. Heat Mass Transf. 47 (17–18) (2004) 3993–4004.
[14] G. Hetsroni, A. Mosyak, E. Pogrebnyak, L.P. Yarin, Heat transfer in micro-channels: comparison of experiments with theory and numerical results, Int. J. Heat Mass Transf. 48 (25–26) (2005) 5580–5601.
[15] G.L. Morini, Y. Yang, M. Lorenzini, Experimental analysis of gas micro-convection through commercial microtubes, Exp. Heat Transfer 25 (3) (2012) 151–171.
[16] T.-Y. Lin, S.G. Kandlikar, A theoretical model for axial heat conduction effects during single-phase flow in microchannels, J. Heat Transf. 134 (2) (2012) 020902.
[17] J.B. Taylor, A.L. Carrano, S.G. Kandlikar, Characterization of the effect of surface roughness and texture on fluid flow—past, present, and future, Int. J. Therm. Sci. 45 (10) (2006) 962–968.
[18] C.-Y. Yang, C.-W. Chen, T.-Y. Lin, S.G. Kandlikar, Heat transfer and friction characteristics of air flow in microtubes, Exp. Therm Fluid Sci. 37 (2012) 12–18.
[19] E.W. Lemmon, M.L. Huber, M.O. McLinden, NIST Standard Reference Database 23: Reference Fluid Thermodynamic and Transport Properties-REFPROP, in, National Institute of Standards and Technology, Standard Reference Data Program, Gaithersburg, 2010.
[20] W.M. Kays, A.L. London, Compact heat exchangers, 1984.
[21] G.P. Celata, M. Cumo, V. Marconi, S.J. McPhail, G. Zummo, Microtube liquid single-phase heat transfer in laminar flow, Int. J. Heat Mass Transf. 49 (19–20) (2006) 3538–3546.
[22] G. Hetsroni, M. Gurevich, A. Mosyak, R. Rozenblit, Drag reduction and heat transfer of surfactants flowing in a capillary tube, Int. J. Heat Mass Transf. 47 (17–18) (2004) 3797–3809.
[23] G. Hetsroni, A. Mosyak, E. Pogrebnyak, L.P. Yarin, Fluid flow in micro-channels, Int. J. Heat Mass Transf. 48 (10) (2005) 1982–1998.
[24] G. Nellis, S. Klein, Heat Transfer, Cambridge University Press, 2009.
[25] S. Baek, C. Lee, S. Jeong, Effect of flow maldistribution and axial conduction on compact microchannel heat exchanger, Cryogenics 60 (2014) 49–61.
[26] R. Barron, Cryogenic Heat Transfer, Taylor & Francis, 1999.
[27] F. Dittus, L. Boelter, Heat transfer in automobile radiators of the tubular type, Univ. Calif. Publ. Eng. 2 (1930) 371.
[28] A. Ewinger, G. Rinke, A. Urban, S. Kerschbaum, In situ measurement of the temperature of water in microchannels using laser Raman spectroscopy, Chem. Eng. J. 223 (2013) 129–134.
[29] C.-Y. Huang, C.-M. Wu, Y.-N. Chen, T.-M. Liou, The experimental investigation of axial heat conduction effect on the heat transfer analysis in microchannel flow, Int. J. Heat Mass Transf. 70 (2014) 169–173.